# SYNTHESIS OF $TiO_2$/GF-Ni HYBRID MATERIALS BY A COMBINED CHEMICAL VAPOR DEPOSITION/RF MAGNETRON SPUTTERING APPROACH

Elena Madalina MIHAI [1,2*], Anca-Ionela ISTRATE[1], Octavian Gabriel SIMIONESCU[1,3], Cristina BANCIU[4], Cosmin ROMANITAN[1], Florin COMANESCU[1], Alexandra BANU[2], L. Monica VECA[1]

*Graphene, and recently 3D graphene networks, have attracted widespread attention in electrocatalysis of wastewater contaminants such as heavy metals, dyes, and solvents, owing to their large surface area and easy regeneration capacity. Even higher* efficiency *is foreseen in the combination with large bandgap $TiO_2$, an outstanding candidate for the photoelectrocatalytic wastewater's decontamination due to its high photocatalytic activity, environmental stability, and nontoxicity. In this context, the 3D graphene networks were obtained by chemical vapor deposition (CVD) on standard commercial nickel foam and the $TiO_2$ thin films were deposited using a reactive radiofrequency magnetron sputtering system from a titanium target in an argon/oxygen gas mixture. The obtained materials were subsequently investigated by X-ray diffraction, field emission scanning electron, and high-resolution Raman spectroscopy. The electrochemical response of the obtained materials has been investigated by cyclic voltammetry. Herein we present the suitability of chemical vapor deposition/RF magnetron sputtering methods to synthesize $TiO_2$/GF-Ni hybrids for electrochemical applications.*

**Keywords**: $TiO_2$, 3D graphene foam, chemical vapor deposition (CVD), magnetron sputtering

## 1. Introduction

Industries spanning from textile and cosmetics to pharmaceutical and food processing are continuously generating wastewater contaminated with organic dyes. To address these environmental challenges, several approaches have been considered, including green chemistry processes, the valorization of reused/recycled materials and the application of different wastewater treatments, as well.

[1] National Institute for Research and Development in Microtechnologies, Bucharest, Romania, e-mail: madalina.mihai@imt.ro
[2] Faculty of Applied Chemistry and Materials Science, University POLITEHNICA of Bucharest, Romania
[3] Faculty of Physics, University of Bucharest, Romania
[4] National Institute for Research and Development in Electrical Engineering ICPE-CA

For the latter approach, considerable attention has been paid to material and technology development, among which photo- and electro-catalysis (PC and EC) have proven appropriate processes. However, they both face several limitations such as low efficiency due to the charge recombination of the photogenerated electron/hole pairs or high energy consumption for the electrochemical degradation of pollutants to biodegradable compounds. Still, in the development stage, a new direction combines heterogeneous photocatalysis with simultaneous electrocatalysis in the so-called PEC (photoelectrocatalysis) process, which allows not only efficient organic pollutants mineralization but, inorganic ion reduction, microorganism inactivation, or $CO_2$ reduction at decreased electrical energy consumption. Various nanomaterials have been explored as photo- and electro-catalyts and their versatility has been extended to several fields [1, 2].

Many metal oxide nanomaterials, such as: $TiO_2$, ZnO, or carbon-based, and graphite carbon nitride (g-$C_3N_4$), in various forms (nanoparticles, quantum dots, nanorods, nanocubes, etc) exhibit photocatalytic activity as it was reported during the last decade. While nanostructured $TiO_2$ was considered the most effective photo-induced catalyst for the oxidation of organic and inorganic pollutants, graphene and its derivatives gained significant attention in the electrocatalytic field [3-5].

Materials engineering in heterogeneous photo/electro-catalysis is mostly associated with the transformations that take place at the molecular level on the catalyst's surface. In other words, the photocatalyst efficiency is correlated with their specific surface area. In this context, nanostructures of large specific surface area have been synthesized but, it is difficult to recover them after the water treatment, unless they are immobilized on a substrate. Moreover, the efficiency is further improved if the substrate is conductive enough to promote charge separation [6,7].

Graphene has a unique two-dimensional structure, with high surface area and conductivity as well as electronic mobility. Consequently, graphene can more efficiently hinder the recombination of electron-hole pairs and thus improve photocatalytic efficiency [8].

Three-dimensional (3D) graphene represents the new architecture of graphene material and has been fabricated by self-assembly [9], templating [10], or chemical vapor deposition (CVD) [11]. In the CVD approach, nickel (Ni) foam was used as the substrate to develop the 3D structure [12,13]. Whereas 2D graphene sheets have conducting pathway restricted to the planar direction, 3D graphene provides multiple channels for fast electron transport. Its excellent electrical conductivity is also due to the absence of intersheet contact resistance. [14].

Herein, we report the investigation on the electrochemical stability of mesoporous $TiO_2$/GF-Ni hybrids. While, the 3D graphene networks (GF-Ni) were obtained by chemical vapor deposition technique (CVD) on standard commercial nickel foam, the $TiO_2$ thin film was deposited using a reactive radiofrequency magnetron sputtering system from a titanium target in an argon/oxygen gas mixture. Structural and morphological investigations revealed the formation of graphene networks, uniformly coated by a thin $TiO_2$ film, consisting of mixed phase nanostructures. Undoubtedly, these types of hybrids have a great potential to function as efficient and reusable electrodes in the photoelectrocatalytic mineralization of organic dyes, as all these 3D structures generate a large surface area of the $TiO_2$ photocatalyst, while the highly conductive GF-Ni favors the separation of photogenerated charges on the $TiO_2$ surface [15-17].

## 2. Experimental details

### *2.1 The growth of 3D Graphene on Ni foam*

The 3D graphene layer was synthesized from methane and hydrogen gas mixture, on open-cell nickel foam catalyst (Gelon LIB, China), using the atmospheric pressure thermal chemical vapor deposition technique in a horizontal furnace (EasyTube 2000, FirstNano, CVD Equipment Corporation, USA). The high purity process gases employed for the graphene growth, methane (>99.9995%), hydrogen (>99.995%), and argon (>99.999%), were purchased from SIAD Romania and used as received. The specified characteristics of the Ni foam are: porosity of 110 ppi (pores-per-inch), thickness of 2.5 mm, and surface density of at least 250 g/m$^2$. The thermal CVD growth of the 3D graphene layer [18] was performed on 1.5 cm×1.5 cm nickel foam substrates, which were ultrasonically cleaned in acetone and isopropyl alcohol prior to being loaded into the preheated (1000 °C) CVD furnace. The specimen, further denoted as GF-Ni, was used in the electrochemical characterizations without other modifications.

### *2.2 Deposition of $TiO_2$ film*

The $TiO_2$ films were deposited by RF Magnetron Sputtering, at room temperature (RT), using the PlasmalabSystem400 (Oxford Instruments, UK). The deposition process was carried out using a titanium (Ti) target (99.5 % purity), argon (Ar – 99.999% purity) as the sputtering gas and molecular oxygen ($O_2$ – 99.999% purity) as the reactive gas. For this set of depositions, the samples oscillated in a parallel plane under the Ti target by a 30° angle (15° left and 15° right) for a better uniformity. The sputtering deposition system and the working mechanism are described in a previous publication [19] and the process parameters used in this work are presented in Table 1. Prior to the RF-sputtering deposition, the as-grown 3D-graphene, underwent surface modification by exposure to UV-ozone at 60 °C for 15 minutes, using an UV-Ozone cleaner

(Novascan Technologies, USA). The electrode obtained at the end of the process was further denoted $TiO_2$/GF-Ni and tested in the electrochemical system without other treatments.

*Table 1.*

**RF Magnetron Sputtering process parameters used for the $TiO_2$ depositions**

| Process pressure (mTorr) | RF power (W) | RF power target density [1] ($W/cm^2$) | Gas flow rate (sccm)[2] | |
|---|---|---|---|---|
| | | | Ar | $O_2$ |
| 10 | 400 | 2.26 | 30 | 2 |

[1] RF power averaged over the entire target surface area; [2] sccm = standard cubic centimeter per minute

### *2.3 Characterization methods*

The elemental composition, morphology, and growth uniformity were ascertained on a high-resolution field-emission scanning electron microscope (FE-SEM) (Nova NanoSEM 630, FEI Company, USA) operated at 10 kV acceleration voltage. The crystal structure of the investigated electrodes was assessed using the Rigaku SmartLab-9 kW X-ray Diffraction System in the grazing incidence (GI-XRD) configuration, operated at 40 kV accelerating voltage with 75 mA applied current, and Cu Kα radiation with $\lambda$ = 0.15406 nm. The angle of the incident beam was fixed at 0.5°, while the detector scanned from 20 to 95°. X-ray reflectivity (XRR) curves were measured in the range $\theta = 0 - 5°$ with a step width of 0.001° and a scan rate equal to 0.2°/min using a medium-resolution set-up with small incident slits (0.5 mm). Raman spectra were carried out on a high-resolution micro-Raman spectrometer (LabRAM HR 800, Horiba, Japan) equipped with a HeNe excitation source (633 nm). The electrochemical characterization of the prepared electrodes was performed through cyclic voltammetry (CV) in 0.1 M $Na_2SO_4$ solution involving an electrochemical workstation Gamry 600 Reference. It has been used a conventional three-electrode cell, with GF-Ni or $TiO_2$/GF-Ni as working electrodes, Ag/AgCl/3M and Pt foil as reference electrode and counter electrode, respectively. The applied potential domain was in the range of -1 V towards 1.5 V *vs.* Ag/AgCl and the scan rate 100 mV/s. The size of the working electrode was 1.4 cm * 1 cm, out of which 1 $cm^2$ was immersed into the electrolyte during the experimental tests.

## 3. Results and discussions

### *3.1 Surface morphology and composition characterizations of the GF-Ni and $TiO_2$/GF-Ni working electrodes*

The working electrodes were prepared on commercial Ni foam, which served as both catalyst and 3D scaffold in the CVD graphene growth with the subsequent physical deposition of the $TiO_2$ layer. SEM surface examination of the GF-Ni specimen (Fig. 1a) reveals the formation of continuous graphene networks

with specific wrinkles and folds, which replicate the structure of the Ni foam. The 30 nm thick $TiO_2$ layer has a granular morphology, comprising nanoparticles aggregated and interconnected into a continuous, uniform film on the GF-Ni substrate (Fig. 1b). In both cases, the graphene foam retains the architecture due to the good mechanical strength.

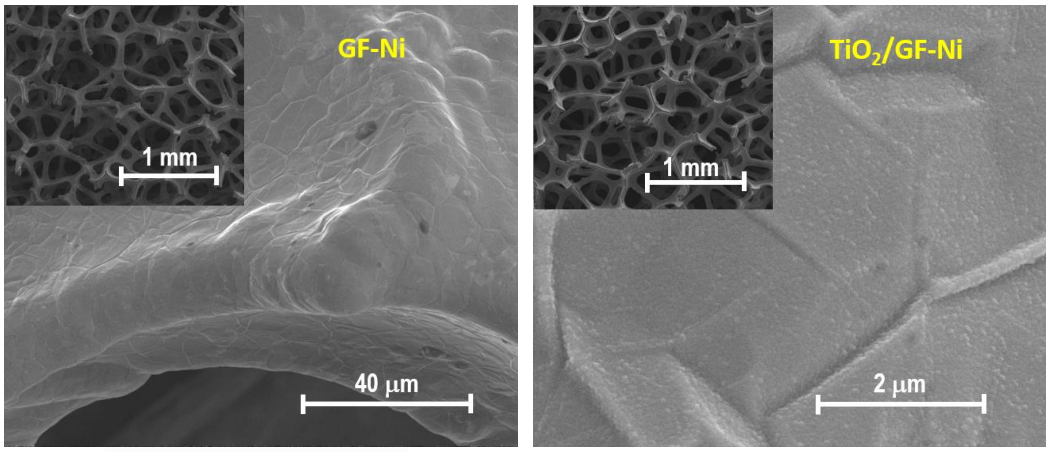


Fig. 1. Low and high magnification SEM images of the as-grown graphene (GF-Ni) working electrodes before (left) and after (right) $TiO_2$ film deposition.

The elemental composition of the two types of electrodes is confirmed by energy dispersive X-rays spectroscopy (EDX), indicating the presence of C, O and Ni in the case of the as-grown GF-Ni and C, O, Ti and Ni in the case of the $TiO_2$/GF-Ni electrode (not shown here). It is worth mentioning that no impurities were observed on the surface of the investigated electrodes.

### *3.2 XRD investigations*

Grazing incidence X-ray diffraction (GIXRD) patterns of GF-Ni and $TiO_2$/GF-Ni are comparatively presented in Fig. 2. In the case of the GF-Ni sample diffraction peaks from the carbon network and the nickel substrate have been noticed, while in the case of $TiO_2$/GF-Ni, the spectrum is similar, except for an additional small feature at 31.51°, which could be as assigned to brookite phase of $TiO_2$. The graphite diffraction peak, highlighted with an olive dashed line, is located at $2\theta = 26.44°$, leading to an interplanar distance $d_{hkl}$ of ~0.36 nm before and after $TiO_2$ deposition, according to Bragg's law: $2d_{hkl}\sin\theta=\lambda$, where $\lambda$ is the wavelength of the incident X-rays. The XRD analysis of $TiO_2$, sputtered under identical conditions on a silicon substrate distinctly indicates the formation of a crystalline phase mixture having the hexagonal symmetry with the following lattice parameters: a=b=0.38 nm and c = 0.92 nm for anatase, and a=b=0.46 nm and c=0.29 nm for rutile (Fig. 2b). The film thickness estimated by X-ray reflectivity on the Si substrate is around 32 nm (not shown here). According to the RIR (Relative Intensity Ratio) method, based on the integral area of the

diffraction peaks, a greater percentage of rutile is involved (i.e. 78%). An evaluation of the crystallinity using the Scherrer formula [20], providing the correlation between the diffraction peak's broadening and the size of the crystalline domains, led to crystalline domains with values of 12.5 nm for rutile and 11.7 nm for anatase, suggesting a good crystallinity for such a small thickness.

Considering the low thickness of the deposited $TiO_2$ layer and the GF-Ni surface morphology, it is likely that the GF-Ni substrate promoted the formation of amorphous titania, probably a consequence of the atomic planes bending due to Ni foam surface morphology. This aspect requires further investigation and will be discussed in a future paper.

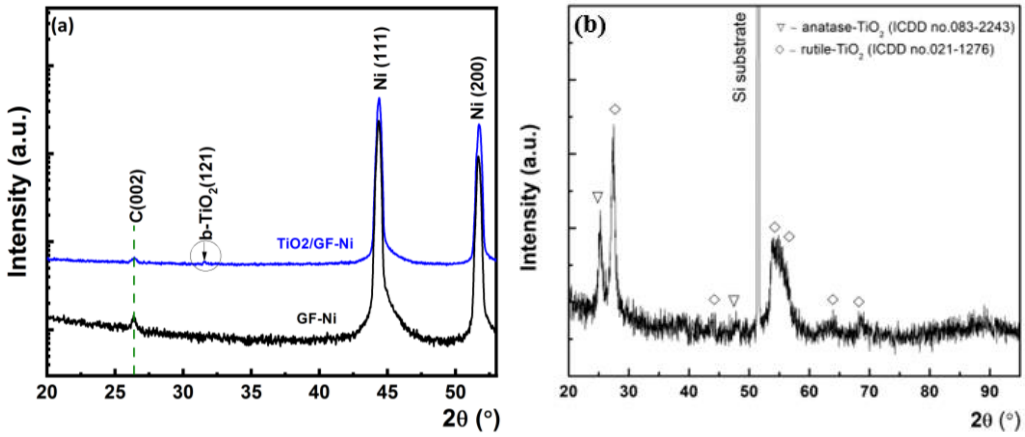


Fig. 2. GIXRD patterns of (a) as-grown graphene (GF-Ni, black line) and $TiO_2$/GF-Ni (blue line), (b) $TiO_2$ deposited on Si.

### *3.3 Raman spectroscopy analysis*

Micro-Raman Spectroscopy was performed to confirm the existence of the as-grown graphene (GF-Ni) and the crystalline phase of $TiO_2$. The Raman spectra of the as-grown graphene multi-layers (GF-Ni) and $TiO_2$/GF-Ni are presented in Fig. 3. Raman spectroscopy of the GF-Ni shows the typical G and 2D peaks as well as the low-amplitude peaks corresponding to the D+D'' and 2D' bands, see Fig. 3 (a). The pointed G band centered at 1582.5 $cm^{-1}$ is a characteristic peak of $sp^2$ carbon structure and reflects the crystallization and symmetry of graphene [21].

The 2D band centered at 2688.9 $cm^{-1}$ is a two-phonon double resonance Raman scattering process [22] and reflects the stack degree of graphene that is a typical symbol to identify the existence of graphene [23]. The absence of the D band, which characterizes the disorder degree of $sp^2$ materials, may indicate either low defect content or that the D peak is invisible because of crystal symmetries (pristine graphene) [24].

The data presented in Table 2 indicate that the as-grown GF-Ni presents the characteristics of a high-quality $sp^2$ material, without defects. Factors supporting this conclusion are the D band's absence, low FWHM of the G peak (close to 20 $cm^{-1}$), as well as its low shift from the 1580 $cm^{-1}$ standard value [25]. After the $TiO_2$ deposition on GF-Ni, the G and 2D peaks' position are almost the same as for the as-grown graphene (G band at around 1582.5 $cm^{-1}$ and 2D band at around 2686.7 $cm^{-1}$) along with disordered induce D (1345.6 $cm^{-1}$) and D'(1622.4 $cm^{-1}$) bands. This fact suggests that the GF-Ni was able to maintain its porous network configuration with small defects induced by the subsequent processing steps performed on the as-grown GF-Ni, as is shown in Table 2. The Raman spectra of the $TiO_2$/GF-Ni electrode exhibit peaks characteristic of $TiO_2$ anatase (147.5 $cm^{-1}$, 526.2 $cm^{-1}$) as well as of rutile $TiO_2$ (445.2 $cm^{-1}$, 614.5 $cm^{-1}$).

The Raman analysis indicates the achievement of high quality and defect-free GF-Ni and suggests the presence of a mixed structure comprised of anatase and rutile phase in the case of the $TiO_2$ thin films.

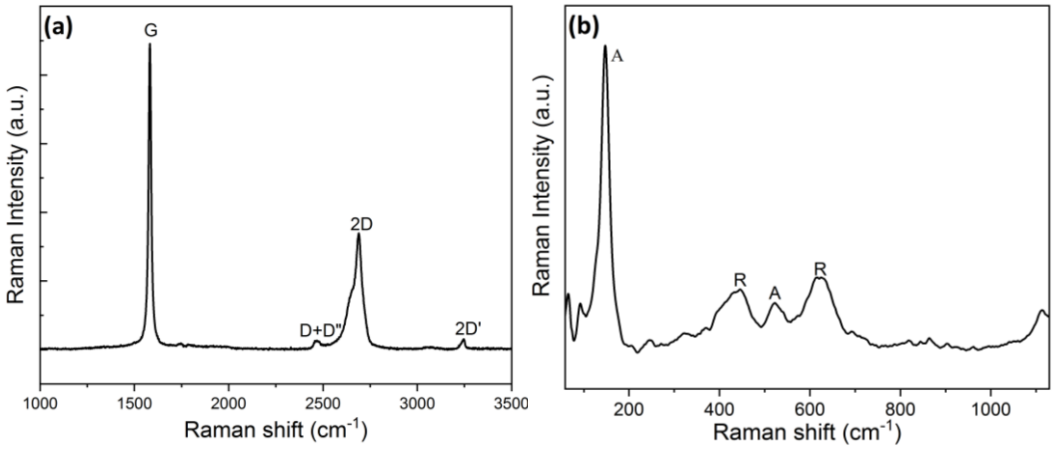


Fig. 3. Raman spectra of the (a) as-grown graphene (GF-Ni) and (b) $TiO_2$/GF-Ni (A = anatase, R = rutile).

*Table 2.*

**Raman shifts of G and the 2D band obtained for GF-Ni, as grown and $TiO_2$/GF-Ni**

| Sample | Peak position | | Intensity ratio | FWHM ($cm^{-1}$) | |
|---|---|---|---|---|---|
| | G | 2D | $I_{2D}/I_G$ | G | 2D |
| GF-Ni, as grown | 1582.5 | 2688.9 | < 1.00 | 16 | 40 |
| $TiO_2$/GF-Ni | 1582.5 | 2686.7 | < 1.00 | 14 | 29 |

### *3.4 Cyclic Voltammetry*

he main objective of the electrochemical characterization of the synthesized material is to verify its electrochemical stability, given that it is

intended to be used as an electrode material in photoelectrocatalysis processes, where the electrode material must not participate in redox reactions. To verify that the synthesized hybrid material is electrochemically active, the technique of cyclic voltammetry in neutral sodium sulfate solution was used, at room temperature and natural aeration conditions.

The electrochemical response of each component of the hybrid material is highlighted by the voltamograms shown in Fig. 4.

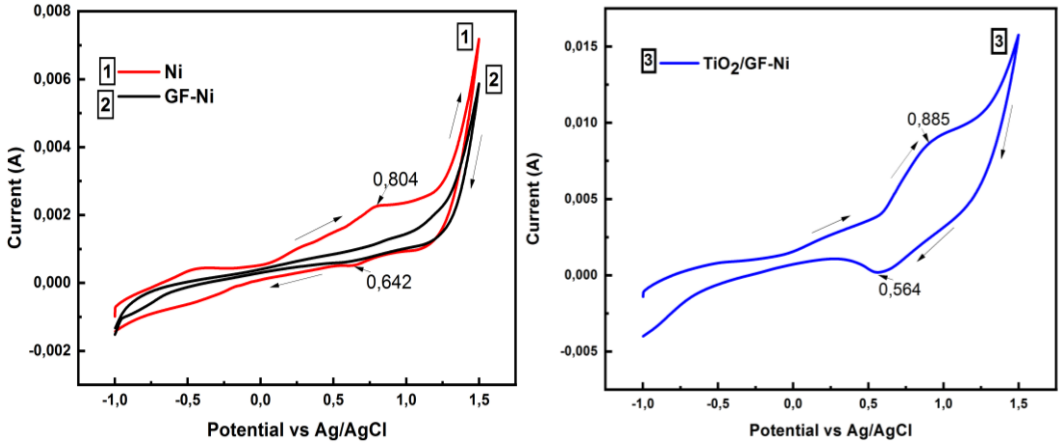


Fig. 4. Cyclic voltammograms obtained on Ni (1 red line), GF-Ni (2 black line) and $TiO_2$/GF-Ni (3 blue line) in 0,1M $Na_2SO_4$ solution at a scanning rate of 100 mV/s in the dark at 25 ºC.

The sensitivity of nickel to the oxygen oxidation reaction takes place at a potential of about 590 mV vs. Ag/AgCl, and the peak of the current is tiny, considering the natural concentration of oxygen in an aqueous solution at 25°C. On the other hand, it is observed that the graphene layer obtained by chemical vapor deposition (curve 2) has good electrical conductivity and it can be used as an electrode material. In addition, the maxima specific for electrochemical processes on nickel electrode in neutral aerated solution disappeared, which is a good indication of the full coverage of the Ni support with the graphene layer.

Instead, in the voltammogram obtained on the hybrid system, $TiO_2$/GF-Ni, (curve 3) these maxima are amplified, values of the currents are about 4 times higher compared to the nickel support, both, in the anodic and in the cathodic fields. In addition, based on the recorded CVs for at least 5 cycles (not shown here), it was noticed a proper electrochemical stability of the synthesized $TiO_2$/GF-Ni hybrid material. Therefore, the obtained hybrid $TiO_2$/GF-Ni material has electrochemical response, it can be used as electrode material and its behavior in the electrochemical oxidation of some specific organic compounds will be studied [26, 27].

## 4. Conclusions

The GF-Ni and $TiO_2$/GF-Ni hybrid materials were developed by a combination of chemical vapor deposition and physical RF-sputtering approach.

Surface morphology characterizations show that even after the deposition of the thin $TiO_2$ film, the sample retains its porous structure, both the graphene and the $TiO_2$ film replicating the structure of the Ni foam. XRD and Raman investigations suggest the presence of a mixed phase structure of anatase and rutile phase of the $TiO_2$ thin films. The electrochemical investigations showed an adequate electrochemical stability of the $TiO_2$/GF-Ni hybrid material. Further experiments related to a more detailed electrochemical investigation of the prepared nanomaterials are scheduled to be presented in a future paper.

**Acknowledgements**

This work was supported by the Operational Programme Human Capital of the Ministry of European Funds through the Financial Agreement 51668/09.07.2019, SMIS code 124705, and by a grant of the Romanian National Authority for Scientific Research and Innovation, CNCS – UEFISCDI, project number - PN-III-P2-2.1-PED-2016-1159 (129PED/2017).

## R E F E R E N C E S

[1] *S.G. Segura, E. Brillas,* Applied photoelectrocatalysis on the degradation of organic pollutants in wastewater, *Journal of Photochemistry and Photobiology C:Photochemistry Reviews,* **vol. 31**, June 2017, pp. 1-35.

[2] *A. Tayel, A. R. Ramadan, O. A. El Seoud,* Titanium Dioxide/Graphene and Titanium Dioxide/Graphene Oxide Nanocomposites: Synthesis, Characterization and Photocatalytic Applications for Water Decontamination, Catalyst, vol. 8, October 2018, pp. 491.

[3] *S. Singh, K. C. Barick, D. Bahadur*, "$Fe_3O_4$ embedded ZnO nanocomposites for the removal of toxic metal ions, organic dyes and bacterial pathogens", in J. Mater. Chem. A, vol. 1, no. 10, Jan. 2013, pp. 3325-3333.

[4] *H. Tju, A. Taufik, R. Saleh, "*Enhanced UV photocatalytic performance of magnetic $Fe_3O_4$/CuO/ZnO/NGP nanocomposites", in J. Phys.: Conference Series. IOP Publishing, **vol. 710**, Jan. 2016.

[5] *A. Halder, M. Zhang, Q. Chi*, "Electrocatalytic applications of graphene–metal oxide nanohybrid materials", in Advanced Catalytic Materials - Photocatalysis and Other Current Trends, In Tech Open, Feb. 2016, pp. 379-414.

[6] *R. Giovannetti, E. Rommozzi, M. Zannotti, C. A. D'Amato,* Recent Advances in Graphene Based TiO2 Nanocomposites (GTiO2Ns) for Photocatalytic Degradation of Synthetic Dyes, *in Catalysts*, **vol. 7**, October 2017, pp. 305.

[7] *S. Al. Jitan, G. Palmisano, C. Garlisi,* Synthesis and Surface Modification of TiO2-Based Photocatalysts for the Conversion of CO2, *in Catalysts*, **vol. 10**, February 2020, pp. 227.

[8] *W. Wang, Z. Wang, J. Liu, Z. Luo, S. L. Suib, P. He, G. Ding, Z. Zhang, L. Sun*, "Single-step one-pot synthesis of $TiO_2$ nanosheets doped with sulfur on reduced graphene oxide with enhanced photocatalytic activity", in Sci. Rep., **vol. 7**, Apr. 2017.

[9] *Y. Xu, K. Sheng, C. Li, G. Shi*, "Self-assembled graphene hydrogel via a one-step hydrothermal process", in ACS Nano, **vol. 4**, no. 7, Jul. 2010, pp. 4324–4330.

[10] *B. G. Choi, M. Yang, W. H. Hong, J. W. Choi, Y. S. Huh*, "3D macroporous graphene frameworks for supercapacitors with high energy and power densities", in ACS Nano, **vol. 6**, no. 5, May 2012, pp. 4020–4028.

[11] *Z. Chen, W. Ren, L. Gao, B. Liu, S. Pei, H.-M. Cheng*, "Three-dimensional flexible and conductive interconnected graphene networks grown by chemical vapour deposition", in Nat. Mater., **vol. 10**, no. 6, Jun. 2011, pp. 424–428.

[12] *U. Patil, S. C. Lee, S. Kulkarni, J. S. Sohn, M. S. Nam, S. Han, S. C. Jun*. "Nanostructured pseudocapacitive materials decorated 3D graphene foam electrodes for next generation supercapacitors", in Nanoscale, **vol. 7**, no. 16, 2015, pp. 6999–7021.

[13] *S. Nardecchia, D. Carriazo, M. L. Ferrer, M. C. Gutierrez, F. del Monte*, "Three dimensional macroporous architectures and aerogels built of carbon nanotubes and/or graphene: synthesis and applications", in Chem. Soc. Rev., **vol. 42**, no. 2, 2013, pp. 794–830.

[14] P. Jaehyeung, Y. Mingdi, "Three-dimensional graphene-TiO2 hybrid nanomaterial for high efficient photocatalysis", in Nanotechnology Reviews, **vol. 5**, no. 4, March 2016, pp. 417-423.

[15] *N. A. Karim, M. S. Alias, H. Yang,* Recent Developments for the Application of 3D Structured Material Nickel Foam and Graphene Foam in Direct Liquid Fuel Cells and Electrolyzers, *in Catalysts*, **vol. 11,** Feb 2021, pp. 279.

[16] *R. Giovannetti, E. Rommozzi, M. Zannotti, C. A. D'Amato,* Recent Advances in Graphene Based TiO2 Nanocomposites (GTiO2Ns) for Photocatalytic Degradation of Synthetic Dyes *in Catalysts*, **vol. 7**, October 2017, pp. 305.

[17] *R.K. Upadhyay, N. Soin,; Ro, S.S.* Role of graphene/metal oxide composites as photocatalysts, adsorbents and disinfectants in water treatment: A review. *RSC Adv. 2014,* **vol. 4**, pp. 3823–3851.

[18] *C. Banciu, M. Lungulescu, A. Bara, G. Sbarcea, D. Patroi, V. Marinescu*, "Graphene grown by chemical vapor deposition on metal foams", in AIP Conf. Proc., **vol. 2206**, Feb. 2020, pp. 050001-1–050001-5.

[19] *C. Banciu, M. Lungulescu, A. Băra, L. Leonat, A. Teișanu*, "3D graphene network investigation by Raman spectroscopy", in Optoelectron. Adv. Mater., **vol. 11**, no. 5-6, May-Jun. 2017, pp. 368–372.

[20] *O. –G. Simionescu, C. Romanitan, O. Tutunaru, V. Ion, O. Buiu, A. Avram*, "RF Magnetron Sputtering Deposition of $TiO_2$ Thin Films in a Small Continous Oxygen Flow Rate", in Coatings, **vol. 9**, no. 7, Jul. 2019.

[21] *A. L. Patterson*, "The Scherrer formula for X-ray particle size determination", in Phys. Rev., **vol. 56**, no. 10, Nov.1939, pp. 978–982.

[22] *Y. Ping, Y. Gong, Q. Fu, C. Pan*, "Preparation of three-dimensional graphene foam for high performance supercapacitors", in Prog. Nat. Sci.-Mater., **vol. 27**, no. 2, Apr. 2017, pp. 177–181.

[23] *J. S. Park, A. Reina, R. Saito, J. Kong, G. Dresselhaus, M. S. Dresselhaus*, "G′ band Raman spectra of single, double and triple layer graphene", in Carbon, **vol. 47**, no. 5, Apr. 2009, pp. 1303–1310.

[24] *L. M. Veca, F. Nastase, C. Banciu, M. Popescu, C. Romanitan,M. Lungulescu, R. Popa*, "Synthesis of macroporous ZnO-graphene hybrid monoliths with potential for functional electrodes", in Diam. Relat. Mater., **vol. 87**, Aug. 2018, pp. 70–77.

[25] *Y.-S. No, H. K. Choi, J.-S. Kim, H. Kim, Y.-J. Yu, C.-G. Choi, J. S. Choi*, "Layer number identification of CVD-grown multilayer graphene using Si peak analysis", in Sci. Rep., **vol. 8**, Jan 2018.

[26] *Y. M. Y. Tang, K. Yin, S. Luo, C. Liu, T. Liu, L. Yang,* Graphene-modified nickel foam electrode for cathodic degradation of nitrofuranzone: Kinetics, transformation products and toxicity, in J. Electrochem. Sci. Eng. **vol. 7**, no. 4, 2017, pp. 201-212.

[27] *N. A. M. Zaid, N. H. Idris*, Enhanced Capacitance of Hybrid Layered Graphene/Nickel Nanocomposite for Supercapacitors, in Scientific Reports, **vol. 6**, pp. 32082.